SANDIA REPORT
SAND2007-6359
Unlimited Release
Printed October 2007

Understanding Amine Catalyzed Silica Polymerization: Diatoms as Bioarchitects

Blake A. Simmons, David B. Robinson, Todd W. Lane, Pamela Lane, Frank Zendejas, Huu Tran, Sylvie Aubry, Erik Spoerke, and Christina A. Bauer

Prepared by
Sandia National Laboratories
Albuquerque, New Mexico 87185 and Livermore, California 94550

Sandia is a multiprogram laboratory operated by Sandia Corporation,
a Lockheed Martin Company, for the United States Department of Energy's
National Nuclear Security Administration under Contract DE-AC04-94AL85000.

Approved for public release; further dissemination unlimited.

Issued by Sandia National Laboratories, operated for the United States Department of Energy by Sandia Corporation.

NOTICE: This report was prepared as an account of work sponsored by an agency of the United States Government. Neither the United States Government, nor any agency thereof, nor any of their employees, nor any of their contractors, subcontractors, or their employees, make any warranty, express or implied, or assume any legal liability or responsibility for the accuracy, completeness, or usefulness of any information, apparatus, product, or process disclosed, or represent that its use would not infringe privately owned rights. Reference herein to any specific commercial product, process, or service by trade name, trademark, manufacturer, or otherwise, does not necessarily constitute or imply its endorsement, recommendation, or favoring by the United States Government, any agency thereof, or any of their contractors or subcontractors. The views and opinions expressed herein do not necessarily state or reflect those of the United States Government, any agency thereof, or any of their contractors.

Printed in the United States of America. This report has been reproduced directly from the best available copy.

Available to DOE and DOE contractors from
U.S. Department of Energy
Office of Scientific and Technical Information
P.O. Box 62
Oak Ridge, TN 37831

Telephone: (865) 576-8401
Facsimile: (865) 576-5728
E-Mail: reports@adonis.osti.gov
Online ordering: http://www.osti.gov/bridge

Available to the public from
U.S. Department of Commerce
National Technical Information Service
5285 Port Royal Rd.
Springfield, VA 22161

Telephone: (800) 553-6847
Facsimile: (703) 605-6900
E-Mail: orders@ntis.fedworld.gov
Online order: http://www.ntis.gov/help/ordermethods.asp?loc=7-4-0#online

Table of Contents

1.0 INTRODUCTION

Current state-of-the-art biomimetic methodologies employed worldwide for the realization of self-assembled nanomaterials are adequate for certain unique applications, but a major breakthrough is needed if these nanomaterials are to obtain their true promise and potential. These routes typically utilize a "top-down" approach in terms of controlling the nucleation, growth, and deposition of structured nanomaterials.[1] Most of these techniques are inherently limited to primarily 2D and simple 3D structures, and are therefore limited in their ultimate functionality and field of use. Zeolites, one of the best-known and understood synthetic silica structures, typically possess highly ordered silica domains over very small length scales. The development of truly organized and hierarchical zeolites over several length scales remains an intense area of research world wide. Zeolites typically require high-temperature and complex synthesis routes that negatively impact certain economic parameters and, therefore, the ultimate utility of these materials. Nonetheless, zeolite usage is in the tons per year worldwide and is quickly becoming ubiquitous in its applications.

In addition to these more mature aspects of current practices in materials science, one of the most promising fields of nanotechnology lies in the advent and control of biologically self-assembled materials, especially those involved with silica[2] and other ceramics such as hydroxyapatite.[3] Nature has derived, through billions of years of evolutionary steps, numerous methods by which fault-tolerant and mechanically robust structures can be created with exquisite control and precision at relatively low temperature ranges and pressures. Diatoms are one of the best known examples that exhibit this degree of structure and control known that is involved with the biomineralization of silica. Diatoms are eukaryotic algae that are ubiquitous in marine and freshwater environments. They are a dominant form of phytoplankton critical to global carbon fixation. The silicified cell wall of the diatom is called the frustule, and the intricate silica structure characteristic of a given species is known as the valve. There are two general classes of diatoms, based on their overall morphologies, the pennate and centric.[4] Diatoms achieve their silicified structures in exact fashion through genetically inspired design rules coupled with precisely directed biochemistry occurring at temperatures ranging from a few degrees Celsius (polar species) to temperatures just over room temperature (tropical species).

Different species of diatoms produce markedly different structures. To start with, there are two basic types of frustule macromorphologies: pennate diatoms display bilateral symmetry and centric diatoms show radial symmetry. There are thousands of permutations of these two basic forms and the micromorphology of the valve can be quite complex with all types of pore arrangements and morphologies (Figure 1.1). The detailed morphology of the cell wall of a given diatom species is reproduced with exactness, because the process is genetically encoded. Three types of cell wall proteins have been identified in diatoms; the frustulins, pleuralins, and silaffins. Frustulins are cell wall proteins that form an organic coat to protect the silica structures from dissolution into the aqueous environment.[5] Pleuralins are associated with a specific subcomponent of the frustule during cell division, and play a role in hypotheca-epitheca development.[6] Silaffins from *Cylindrotheca fusiformis* are short chain-length peptides that play a direct role in the silica polymerization process, and possess unique biochemical post-translation functionalization.[7, 8] Larger proteins with silaffin activity have recently been described in *Thalassiosira pseudonana*.[9] Frustulins and pleuralins play no role in silica polymerization or

structure formation in diatoms, whereas the silaffins are one of the primary polymerization determinants. In addition to the silaffins, a class of long-chain polyamines associated with diatom silica has been identified, and shown to also be involved in the silica polymerization process.[10] The silaffins and polyamines are likely to be the two major determinants of silica polymerization in diatoms. Their involvement in the formation of higher order structure is unclear; there have been suggestions that they self-assemble in various combinations to form the final frustule structure[8,11,12] but these are highly speculative as there is no substantial data to support this. It is clear from a long history of electron microscopic observations[13] that a major determinant of silica structure in diatoms is generated by growth and molding of the silica deposition vesicle (SDV), the specialized intracellular compartment were the frustule is made.

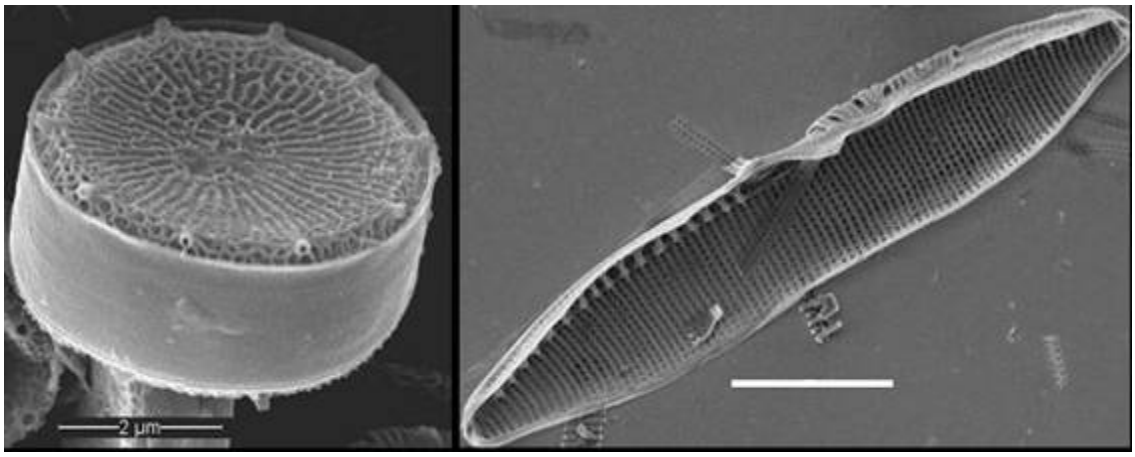

Figure 1.1. Electron micrographs that represent the two basic frustule types as a function of diatom species. At left, *Thalassiosira pseudonana*, scale bar = 2 µm, at right, *Nitzschia alba*, scale bar 5 = µm.

Diatoms are the focus of research activity on several fronts, including the processes by which their distinct silica frustules are formed. Within the diatom cell the frustule is formed inside a membrane-bound organelle called the Silica Deposition Vesicle (SDV). Diatoms actively transport silicon as silicic acid into the cell via silicic acid transport (SIT) proteins, and then into the SDV. Silaffins and polyamines are involved in the silica polymerization process, and these components and derivatives of them have been used *in vitro* to form nanostructured or nanopatterned silica, using a variety of techniques. Different combinations of silaffins and polyamines[8], and polymerization reactions carried out under different pHs or in the presence of shear flow, have given rise to different silica morphologies *in vitro.*[14] The use of these biological entities in conjunction with different patterning techniques are a growing area of research. One of the most intriguing results was the development of nanopatterned silica in a photopolymerized process involving cationic polypeptides.[15] Various biomimetic environments have been developed that employ dendrimers[16] and/or polyamines.[17] These results are very preliminary and have only produced discrete nanoparticles of silica with varying degrees of success and control. Observations utilizing electron microscopy and varied inhibition experiments have shown that diatom silica structure is largely formed by controlled movements and passive molding of the SDV.[13]

2.0 IMPACT OF AMINE STRUCTURE ON BIOINSPIRED SILICA POLYMERIZATION

2.1 Introduction

Inspired by the ability of diatoms to grow beautiful and complicated skeletons of silica under conditions near room temperature and neutral or mildly acidic pH,[18,19] much recent work has been reported on the chemical approach these organisms use to achieve this, and on artificial schemes to produce similar results. While other methods for growth of templated silica exist,[20] no technology exists for making controlled, complex three-dimensional structures on the nanometer and micrometer scales under mild synthetic conditions. This has been the motivation of the previous work: such a technology would open new paths toward sophisticated micro- and nanoscale mechanical, optical, or electronic devices, as well as media for chemical reactions and separations.[21]

In diatoms, silica grows at the interfaces of precursor-containing vesicles with the help of proteins. In the diatom *Cylindrotheca fusiformis*, these proteins are known to contain lysines modified with oligo(1-methylazetane), as shown in Figure 2.1, terminated by a primary amine, as well as methylated lysines.[22,23,24,25] Other structures with intriguing similarities and differences have been observed in other species.[262728] This has led others to study the ability of various amines to react with silica precursors such as silicic acid buffered by borate, tris(hydroxymethylaminomethane), or phosphate;[29,30,31,32] catecholate complexes;[33] or partially hydrolyzed alkoxysilane.[34,35,36,37,38] The amines previously studied include large molecules such as modified peptides extracted from diatoms,[24,32,39] polyamines such as poly(allylamine) and polylysine,[29,40,41,42,43,] dendrimers,[44] oligo(N-methyl azetane)s,[33] and oligo (ethylene diamine)s and/or spermine and spermidine.[34,45] Studies of smaller molecules include long-chain diamines,[37,46] functional monoamines,[36] amino acids,[31,47] and cyclic diamines.[35] Quaternary ammonium-containing surfactants[38,48,49] or polymers[50,51] have also been studied. Most of these studies have focused on producing silica with mesoscale order, and only a few have attempted systematic studies relating structure to reactivity. In an attempt to clarify the complex patterns observed, we seek to identify a minimal amine moiety necessary to accelerate silica condensation, and make small structural variations to understand why this may be so. To accomplish this, we have screened a few monoamines and range of short diamines, varying chain length, degree of alkylation, and presence of adjacent functional groups. From this, we have identified structural features that result in significant changes to reactivity. This may help clarify the mechanism by which amines interact with silicate to promote condensation in diatoms, and facilitate creation of structured silica in artificial settings.

2.2 Experimental Details

All materials were obtained from Aldrich and used as received, unless otherwise specified. Solutions of the amines under study were titrated to pH 7.5 with hydrochloric acid, giving a final concentration of 62.5 mM (no titration was necessary for quaternary ammonium compounds). Buffered silicic acid solutions were prepared by neutralizing 0.5M aqueous sodium metasilicate (MP Biomedicals, nonahydrate) by addition to 1.33 equivalents of phosphoric acid in a volume of water necessary to give a final concentration of 90 mM silicate (*i.e.*, after the amine is added). Both reagents were cooled in an ice bath before mixing, and then warmed in a room-temperature

water bath for 5 minutes, resulting in a solution of pH 7. These solutions were prepared immediately before use. An initial absorbance spectrum was taken from 400 to 500 nm on a Shimadzu UV-2501 spectrometer. Enough amine was added to achieve a 5 mM concentration (10 mM for monoamines) and the absorbance was measured as a function of time thereafter. The poly(methyl methacrylate) cuvettes were shaken to achieve initial mixing. Settling was sometimes observed when long time intervals elapsed between measurements, in which case the cuvette was inverted once before measurement. Absorbance spectra increased gradually with decreasing wavelength. The absorbance at 480 nm was taken as a measure of turbidity. Scanning electron microscopy specimens were prepared by washing 0.1 mL gel with 0.4 mL deionized water three times by spinning for 15 minutes at 5000 rpm in a Millipore Microcon filtration tube with a 30kDa molecular weight cutoff, followed by slow drying under reduced pressure, and sputtering with 2 nm gold-palladium alloy. Specimens were examined at 2 and 5 kV on a Hitachi S-4500 microscope.

Preparation of quaternary ammonium dimers

N,N'-dibenzyl N,N,N',N'-tetramethyl propanediammonium bromide (P22 Bz): 2.0 mmol N,N,N',N'-tetramethyl diaminopropane and 4.0 mmol benzyl bromide were added dropwise to 18 mL acetonitrile in a room-temperature water bath with stirring, and left overnight. The precipitated product was filtered, rinsed with ethyl acetate, in which the reactants and monoammonium salts are soluble, and dried under vacuum. Ethane, butane, DABCO, and DMAP versions (E22 Bz, B22 Bz, DABCO Bz, DMAP Bz) were prepared similarly, as were products of E22 with allyl bromide (allyl E22), and products with ethyl bromoacetate (P22 AcOEt, E22 AcOEt, DABCO AcOEt). To induce precipitation of P22 AcOEt, most of the solvent was removed under vacuum and ethyl acetate was added. DABCO is 1,4-diazabicyclo[2.2.2]octane. DABCO Bz was prepared in N,N-dimethylformamide, and the product was treated with hot isopropanol. DMAP is 4-(dimethylamino)pyridine; its reaction product is a monosubstituted pyridinium salt. E22 Bz δ_H (500 MHz, D_2O, HDO = 4.66): 3.1 (s, 6H, N-CH_3); 3.9 (s, 2H, N-CH_2); 4.6 (s, 2H, benzyl); 7.46 (d, 4H, aryl); 7.53 (m, 1H, aryl). Allyl E22: 3.1 (s, 6H, N-CH_3); 3.8 (s, 2H, N-CH_2); 4.0 (d, 2H, allyl N-CH_2); 5.7 (t (asym.), 2H, allyl CH_2); 6.0 (sept, 1H, allyl C*H*). P22 Bz: 2.36 (pent, 1H, central -CH_2-); 3.0 (s, 6H, N-CH_3); 3.3 (t, 2H, N-CH_2); 4.47 (s, 2H, benzyl); 7.45 (d, 4H, aryl); 7.5 (m, 1H, aryl). B22 Bz: 1.86 (2H, central CH_2); 2.96 (6H, N-CH_3); 3.3 (2H, N-CH_2); 4.4 (2H, benzyl); 7.47 (4H, aryl); 7.5 (1H, aryl). DABCO Bz: 3.88 (s, 6H, bridging); 7.47 (m, 4H, aryl); 7.53 (m, 1H, aryl); benzyl H probably exchange with solvent. P22 AcOEt: 1.22 (3H, ethyl); 2.3 (1H, central CH_2); 3.25 (6H, N-CH_3); 3.6 (2H, N-CH_2); 4.22 (2H, ethyl); 4.3 (2H, acyl). E22 AcOEt: 1.22 (t, 3H, ethyl); 4.25 (s, 6H, N-CH_3); 4.24 (q, 2H, ethyl); 4.21 (2H, bridging); 4.37 (2H, acyl). DABCO AcOEt: 1.22 (3H, ethyl); 4.24 (2H, ethyl); 4.25 (6H, bridging); 4.54 (2H, acyl). DMAP Bz: 3.06 (6H, N-CH_3); 5.18 (2H, benzyl); 6.73 (2H, *m*-py); 7.24 (2H, aryl); 7.34 (3H, aryl); 7.91 (2H, *o*-py).

p-phenylenedimethylenebis(triethylammonium bromide) (X33): 1.7 mmol α,α'-dibromo-p-xylene was dissolved in 18 mL acetonitrile with stirring in a 40 C water bath. 3.4 mmol triethylamine was added dropwise. A precipitate formed within 5 minutes, and the reaction was left to stir for an additional hour. The product was cooled to room temperature and isolated as above. A pyridinium version XPy was prepared similarly. X33 δ_H (500 MHz, D_2O, HDO = 4.66): 1.3 (t, 9H, ethyl); 3.15 (q, 6H, ethyl); 4.39 (s, 2H, benzyl); 7.55 (s, 2H, aryl). XPy: 5.76 (2H, benzyl); 7.45 (2H, aryl); 7.99 (2H, *m*-py); 8.47 (1H, *p*-py); 8.8 (2H, *o*-py).

p-phenylenedimethylenebis(2-acetamidoethyl dimethylammonium bromide) (XE20 Ac): 2.0 mmol N,N-dimethyl ethanediamine was added dropwise to 2.0 mmol acetic anhydride and 2.0

mmol diisopropylethylamine in 8 mL acetonitrile while stirring in a room-temperature water bath. This was left to stir overnight. This was added without purification to 1.0 mmol α,α'-dibromo-*p*-xylene in 12 mL acetonitrile at 40 C, following the procedure for X33 thereafter. The N-methyl 2-acetamidoethyl version XE21 Ac and the 3-acetamidopropyl version XP20 Ac were prepared similarly. XE20 Ac δ_H (500 MHz, D_2O, HDO = 4.66): 1.9 (s, 3H, acetyl); 1.96 (s, 2H, acetate); 3.0 (s, 6H, N^+-CH_3); 3.4 (t, 2H, NH-CH_2); 3.65 (t, 2H, N^+-CH_2); 4.52 (s, 2H, benzyl); 7.61 (s, 2H, aryl). XE21 Ac: 2.03 (s, 3H, acetyl); 3.03 (s, 9H, N-CH_3); 3.44 (2H, NMe-CH_2); 3.83 (2H, N^+-CH_2); 4.57 (2H, benzyl); 7.64 (2H, aryl). XP20 Ac: 1.88 (3H, acetyl); 2.01 (2H, central propylene CH2); 2.98 (6H, N-CH_3); 3.19 (2H, NH-CH_2); 3.23 (2H, N^+-CH_2); 4.48 (2H, benzyl); 7.58 (2H, aryl).

Acetamides P22 AcNHPr, E22 AcNHPr, DABCO AcNHPr, and P22 AcPrd were prepared by reacting P22 AcOEt, E22 AcOEt or DABCO AcOEt with 10 uL/mg neat propylamine or pyrrolidine overnight on a 37 C shaker. P22 AcNHPr dissolved; excess amine was decanted from the others. P22 AcPrd was sonicated briefly in acetonitrile, which was decanted, removing impurities. Products were dried under nitrogen and then under vacuum. P22 AcNHPr δ_H (500 MHz, D_2O, HDO = 4.66): 0.8 (t, 3H, propyl CH_3); 1.43 (sext, 2H, propyl CH_2-CH_2-CH_3); 2.31 (pent, 1H, central CH_2); 3.11 (t, 2H, propyl NH-CH_2); 3.21 (s, 6H, N^+-CH_3); 3.56 (t, 2H, bridging N^+-CH_2). E22 AcNHPr: 0.8 (t, 3H, propyl CH_3); 1.43 (sext, 2H, propyl CH_2-CH_2-CH_3); 3.11 (t, 2H, propyl NH-CH_2); 3.28 (s, 6H, N^+-CH_3); 4.24 (s, 2H, bridging N^+-CH_2). DABCO AcNHPr: 0.8 (t, 3H, propyl CH_3); 1.43 (sext, 2H, propyl CH_2-CH_2-CH_3); 3.11 (t, 2H, propyl NH-CH_2); 4.21 (s, 6H, bridging N^+-CH_2). P22 AcPrd ^{1}H NMR: 1.8 (pent, 2H, ring N-CH_2-CH_2); 1.9 (pent, 2H, ring N-CH_2-CH_2); 2.25 (pent, 1H, central CH_2); 3.25 (s, 6H, N^+-CH_3); 3.35 (d, 2H, N^+-CH_2); 3.4 (t, 2H, ring N-CH_2); 3.66 (t, 2H, ring N-CH_2). Acyl protons do not appear in these spectra, presumably due to exchange with the solvent.

2.3 Results and Discussion

In an effort to make this work relevant to the chemistry of diatoms, we use a reactant comparable to the material found in natural waters and accumulated by the organisms, silicic acid (the lowest pKa of which is 9.8). Sodium metasilicate, $NaSiO_3$, dissolves in water to form NaH_2SiO_4, which can be acidified. This must be done with care, because silicic acid spontaneously condenses to form a gel at near-neutral pH, especially at high concentrations or if unbuffered. A phosphate buffer was used, which establishes mild pH, and affords a solution stable on a timescale of hours while allowing amine-accelerated reactions to occur on a rapid but measurable timescale. Measurements presented here are at pH 7 unless otherwise noted. The enhanced stability of the silicic acid in these solutions is likely due to both buffering and complexation,[52] and this is an important factor in the chemistry of condensation.[32] This is also suspected to be the case inside a diatom,[53] where silicic acid concentrations are known to be much higher than in seawater.[54] The actual pH in the regions of silica deposition within a diatom is expected to be as low as 5,[55] but for reasons made apparent below, this would not be ideal conditions for the full range of our experiments. A disadvantage of the use of phosphate is that it interferes with the colorimetric molybdate test.[56] However, the turbidity of the solution increases during gelation, and this property has previously been shown to be useful for rapid screening of silicate reactivity under various conditions.[32,57] We have found that 90 mM is a silicic acid concentration that results in an optically uniform gel over a wide range of amines used, and reacts on an appropriate timescale for rapid reactivity screening.

To identify the simplest effective analog of the oligo(N-methylazetane) catalysts present in diatoms, we examined the reactivity of silicic acid with a variety of mono- and diamines and quaternary ammonium salts. The absorbance curves of representative monoamines are illustrated in Figure 2.2. All amines produce more rapid turbidity increases and higher final turbidities than a control sample using an equal volume of deionized water in place of the amine. A clear increase is seen as the amine is more alkylated, although no major change is seen as quaternary alkyl chains become longer than ethyl.

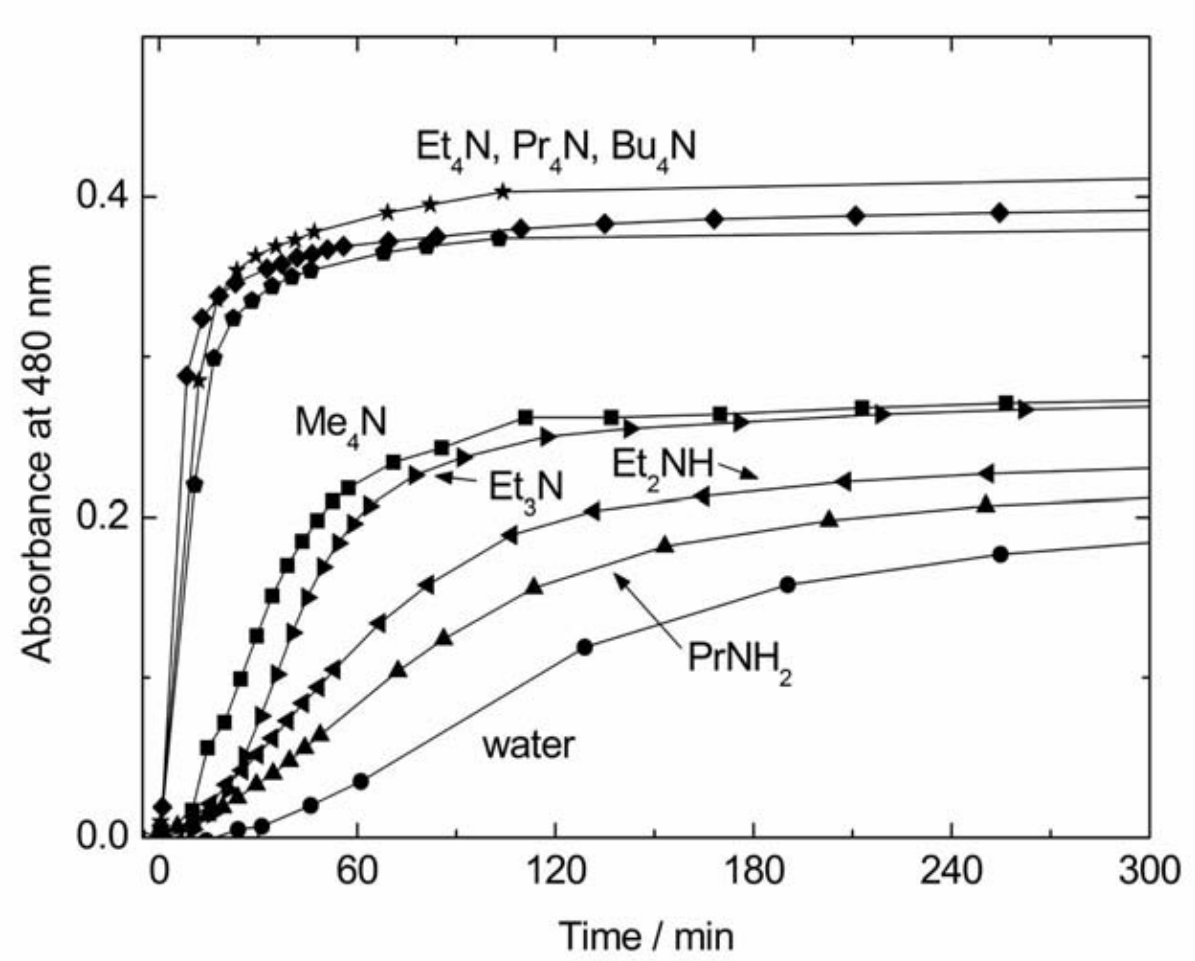

Figure 2.2: Reactivity of phosphate-buffered silicic acid induced by various ammonium salts, as measured by monitoring absorbance at 480 nm as a function of time after preparation of a solution of 90 mM sodium metasilicate, 120 mM phosphoric acid, and 10 mM of a specified alkylammonium chloride (bromide, in the case of Et4N). The top three are listed in decreasing order of their initial slopes.

To study substances that bear closer structural resemblance to the oligoamines found in diatoms, we studied a similar series of diaminoethanes and diaminopropanes, varying the number of N-methyl groups on each, as shown in Figure 2.3. We abbreviate the names of each amine by indicating "E" for diaminoethane, "P" for diaminopropane, or "B" for diaminobutane, followed by a digit indicating the number of methyl groups on each amine. The structures of those labeled in the figures appear in Table 2.1. All combinations of 0-2 methyl groups were tested for E and

P, and one B substance was tested. Again, increased alkylation results in significant increases in the rate of reaction and final turbidity; there is a clear correlation between reactivity and the number of methyl groups on a diamine. In most cases, the reactivity is near that of similarly alkylated monoamines, but diamines with more than three methyl groups are at least as reactive as tetraethylammonium. P22 is dramatically more reactive than E22, but no major change is seen between P22 and B22. The oligoamine identified in *C. fusiformis* bears a strong resemblance to P22, which could be considered a small model compound for this larger structure.

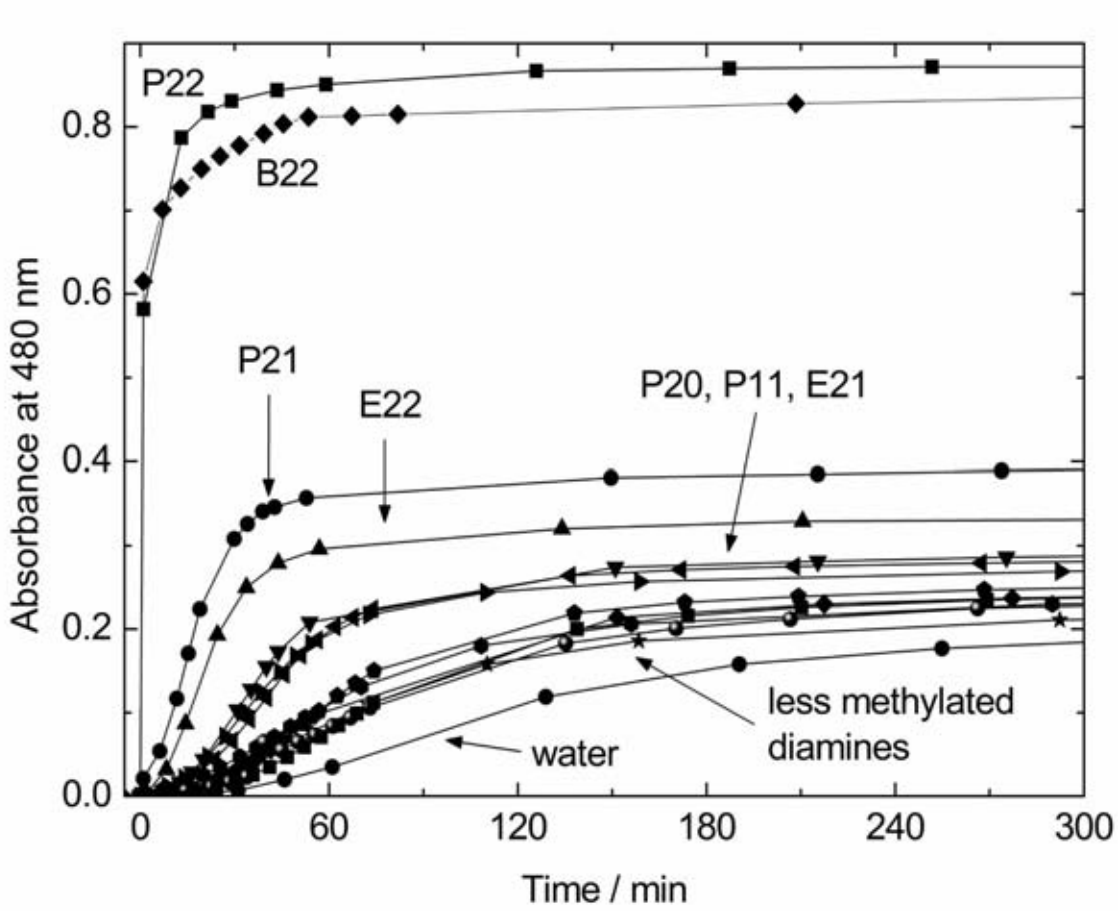

Figure 2.3: Reactivity of phosphate-buffered silicic acid induced by various diamines, as measured by the same method as in Fig. 2, but with 5 mM of a specified diamine from a stock solution titrated to pH 7.5 by hydrochloric acid. The structures of the diamines are described in Table 1. The three similar diamines are listed from most to least turbid.

Table 2.1 Structures of linear diamines.

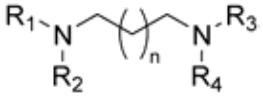

n	R_1	R_2	R_3	R_4

E21	0	CH_3	CH_3	CH_3	H
E22	0	CH_3	CH_3	CH_3	CH_3
P11	1	CH_3	H	CH_3	H
P20	1	CH_3	CH_3	H	H
P21	1	CH_3	CH_3	CH_3	H
P22	1	CH_3	CH_3	CH_3	CH_3
IP11	1	$CH(CH_3)_2$	H	$CH(CH_3)_2$	H
B22	2	CH_3	CH_3	CH_3	CH_3

The second pKa values of some diamines approach that of the second pKa values of phosphate, so it could be suggested that reactivity is related to acid-base chemistry of the amine. Our titration data showed that the second pKa of P00 is 9.0, and that of E00 is 7.1, and that of the others could be found by subtracting 0.5 for each tertiary amine (see supporting information). Increased methylation results in lower pKa, but more importantly, an increased number of methylenes between the amines raises the second amine pKa, which opposes the reactivity trend. Furthermore, the pKa depends on which amines the methyl groups are on, while the reactivity does not; as Figure 2.3 shows, the reactivity induced by P20, with a pKa of 8.5, is nearly identical to that of P11, with a pKa of 9.0. It is apparent from these results that the reactivity is not simply a buffering effect by the amine. More alkylated amines are also more nucleophilic, but if this were important, we would again expect P20 to be more reactive than P11. Also, both are essentially fully protonated under the conditions used, which would inhibit this property. This and the observed effectiveness of quaternary ammonium suggest that nucleophilicity, considered important in the case of alkoxysilanes,[34] is not important to the mechanism of accelerated condensation of phosphate-buffered silicic acid.

Instead, we expect the mechanism to be related to electrostatic interactions. While silicic acid is essentially fully protonated at neutral pH, its oligomers (which form spontaneously) have lower pKa values.[58,59] This creates the possibility of ionic interactions with cationic amines. As observed here and is well known, the condensation of silicic acid is very sensitive to concentration.[58] To explain why polylysine behaves differently from lysine with respect to silicic acid, Coradin *et al.* have suggested that neighboring cationic amines help to preconcentrate anionic oligomers in a configuration favorable for reaction.[40] We believe that alkylation of an amine enhances this effect by decreasing solvent interactions with it,[60] favoring association with silicate oligomers. A version of P11 containing isopropyl side groups instead of methyl groups ("IP11") reacts like P21 instead of P11. Dependence on such subtle structural effects suggests that close-range association between the diamine and silicate occurs. Our results warrant further study of diamines, including study of the approach presented here, by methods such as nuclear magnetic resonance to learn about their configuration while interacting with silicate.[34,54]

The above results lead to the question of the reactivity of bis(quaternary ammonium) salts. Such structures would depart from those observed in diatoms, but approach the field of gemini surfactants,[61] which have been applied to silica in conventional sol-gel syntheses and surface studies.[62] These are easily synthesized by reaction of a tertiary amine with an alkyl bromide. When a highly reactive substrate is used, such as benzyl bromide, this proceeds quickly and cleanly enough to facilitate rapid screening of a variety of products. We observe from Figure 2.4 that, whereas P22 is about twice as effective as tetraethylammonium at inducing turbidity, its benzylated version is twice again as effective, and the reaction in both the P22 and P22 Bz cases

is very fast compared to the timescale of the experiment. As seen for the tertiary amines, the propyl spacer is optimal among the three measured. A test using allyl bromide instead of benzyl bromide shows that the results are not unique to benzyl derivatives.

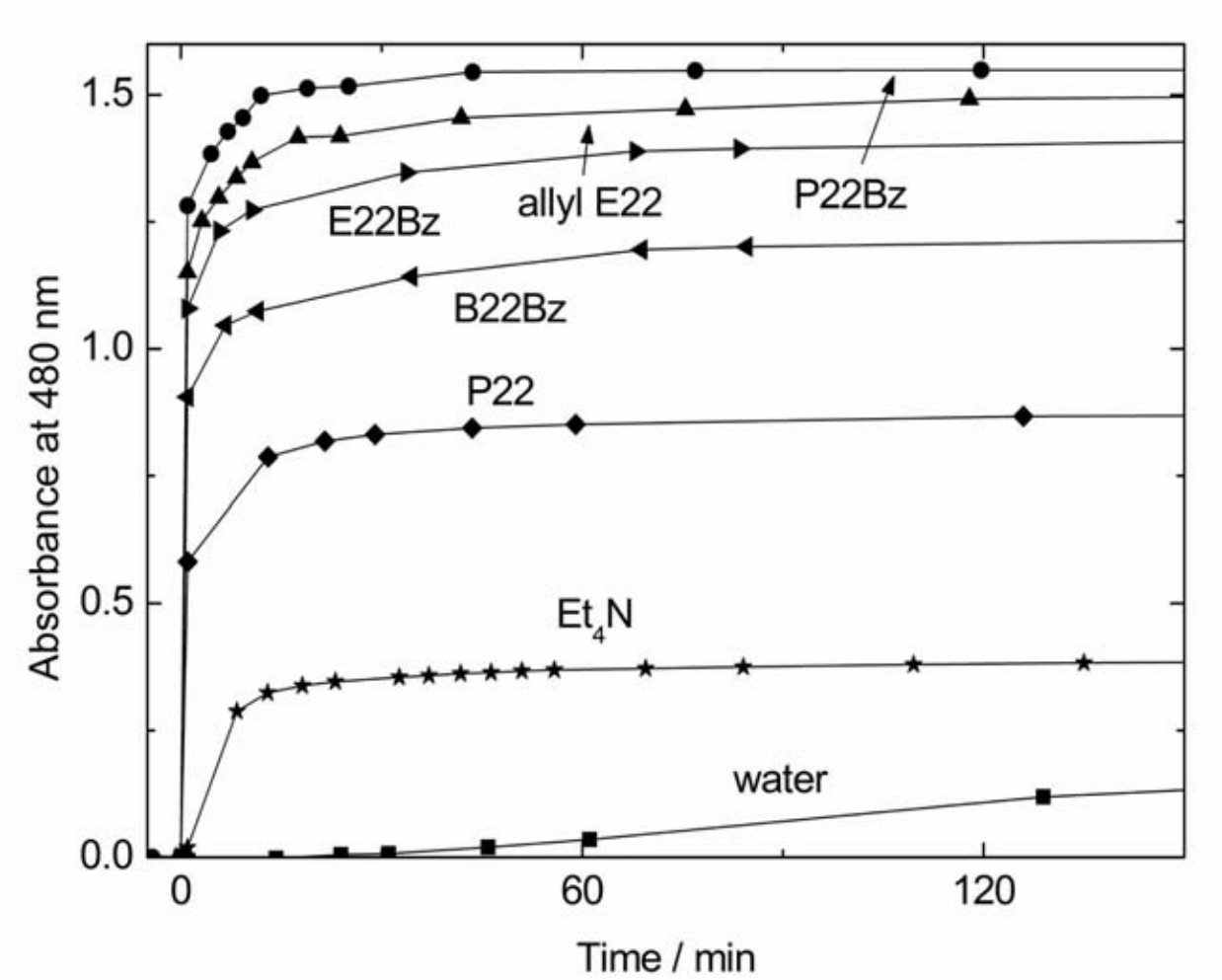

Figure 2.4: Comparison of the reactivity of phosphate-buffered silicic acid induced by bis(quaternary ammonium) salts to previously discussed amines, as measured by the same method as in Fig. 2.3 (quaternary salts were not titrated). The structures of the diamines are described in Tables 2.1 and 2.2. Et4N is tetraethylammonium bromide.

Table 2.2 Structures of bis(quaternary ammonium) bromide salts with aliphatic spacers.

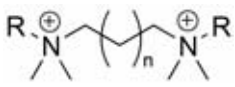	
E22 (n=0), P22 (n=1), B22 (n=2)	DABCO
	R = [a]

E22 Bz P22 Bz B22 Bz DABCO Bz	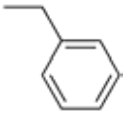
allyl E22	
E22 AcOEt P22 AcOEt DABCO AcOEt	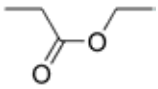
E22 AcNHPr P22 AcNHPr DABCO AcNHPr	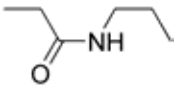
P22 AcNHPrd	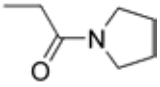

[a] R groups attach through the leftmost bond.

Table 2.3 Structures of pyridinium bromide salts and bis(quaternary ammonium) bromide salts with aromatic spacers.

Viologen: R = methyl or benzyl	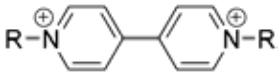
Diquat	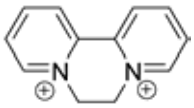
DMAP Bz	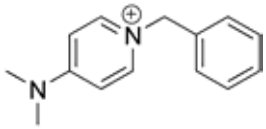
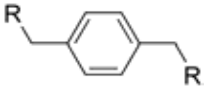	R = [a]
XPy	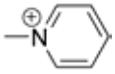
X33	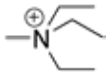
XE20Ac (n=0, R_1=H) XE21Ac (n=0, R_1=CH_3) XP20Ac (n=1, R_1=H)	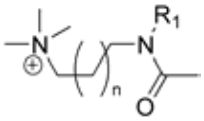

[a] R groups attach through the leftmost bond.

Conformational constraints in quaternary salts further enhance reactivity. In Figure 2.5, benzylated DABCO shows significantly more reactivity than its less constrained analog, E22 Bz. A diammonium salt with a xylyl spacer behaves similarly to those with alkyl spacers, but when the salt is composed of conformationally constrained pyridinium instead of alkylammonium, the resulting turbidity is substantially higher. In fact, very high turbidities are rapidly attained with

the use of alkylated 4,4'-bipyridinium salts (viologens) or an ethylene-bridged 2,2'-bipyridinium salt (diquat). Benzyl viologen becomes twice as turbid as P22 Bz.

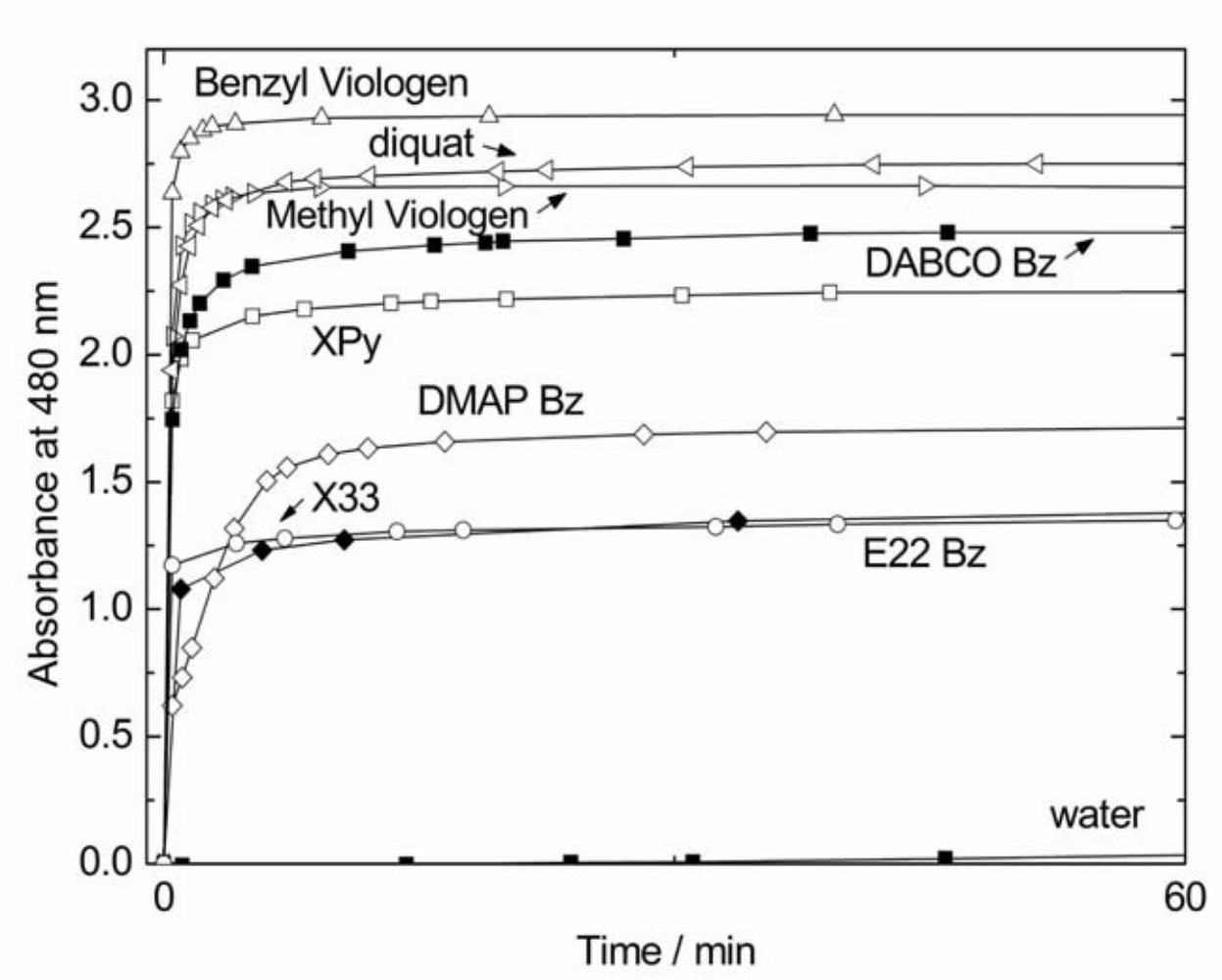

Figure 2.5: Reactivity of phosphate-buffered silicic acid induced by conformationally constrained bis(quaternary ammonium) salts, as measured by the same method as Fig. 2.4. Chemical structures are shown in Tables 2.2 and 2.3.

For the amines in Figures 2.2 and 2.3, a reaction resulting in higher turbidity also approaches that value more quickly, so both features of the data can be taken as qualitative measures of reactivity. Consistent correlation between the speed of the reaction and the final turbidity was observed. In the cases of P22 and most quaternary salts, the reaction occurs on the timescale of mixing, and we have assumed that this correlation still holds. However, DMAP Bz, which contains both a pyridinium and a tertiary amine, shows quite high turbidity but slow kinetics compared to others in Figure 2.5, casts some doubt on its generality. To gain an understanding of the correlation between reactivity and turbidity, electron micrographs were obtained on representative dried gels. These appear in Figure 2.6. The gels are composed of fused particles, the size of which increases for more rapidly reacting amines. The roughness and porosity of the resulting materials also increases. Particles can become larger if their growth is rapid enough to

outpace nucleation of nearby particles, and larger particles scatter more light, so the connection between reactivity and turbidity is plausible.

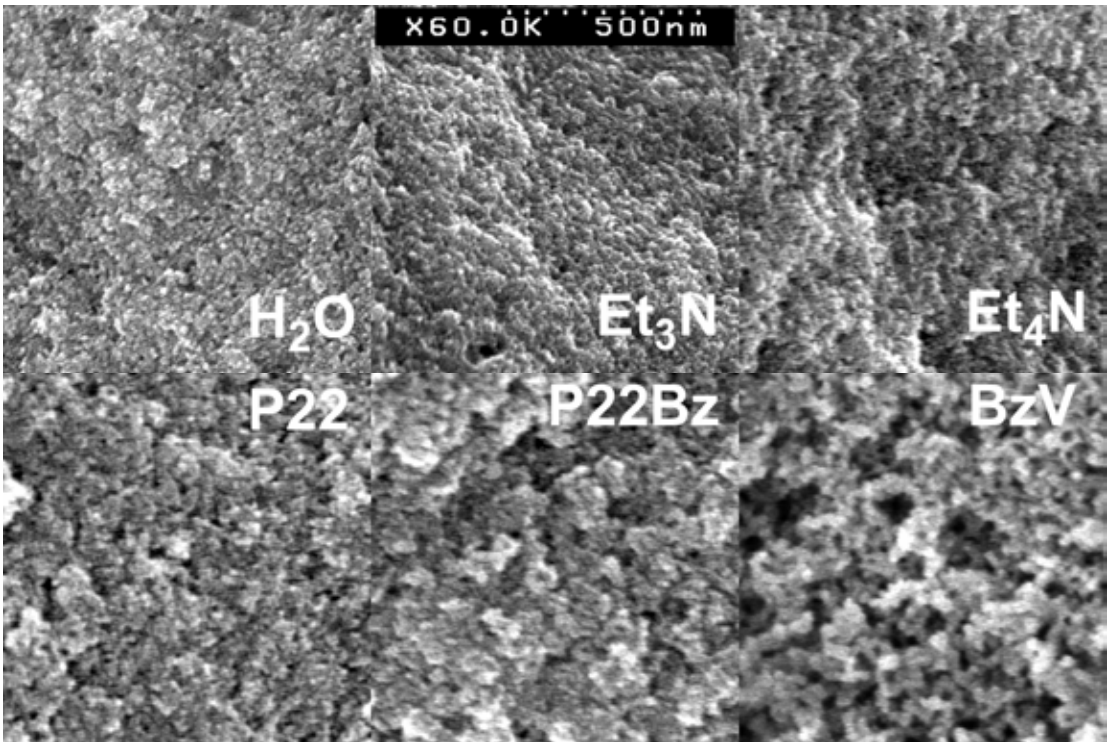

Figure 2.6: Scanning electron micrographs of dried gels formed using representatives of the several types of amines studied. Top row, from left to right: control (H2O), triethylammonium chloride (Et3N), tetraethylammonium bromide (Et4N); bottom row, from left to right: P22, P22 Bz, and benzyl viologen (BzV). The scale bar shown in the upper center of the figure applies to all the SEM images.

To gain further evidence for this correlation, several reactions were run at pH 6 (by increasing the phosphoric acid ratio from 1.33 to 1.78) and the rates were seen to slow down to measurable values (see supporting information). Under these conditions, methyl viologen reached 60 percent of its final value in 3 minutes, P22 Bz in 10 minutes, and P22 in 65 minutes, suggesting that the correlation still holds in most fast reactions. The decrease in reaction rate with decreasing pH helps corroborate the involvement of anionic silicate species in the reaction. Constrained quaternary ammonium salts may be more reactive by providing fixed targets to which silicate can associate more closely and for longer periods of time. This hypothesis could be addressed by spectroscopic methods, as noted above, and by molecular dynamics simulation. The pH inside the silica deposition vesicle of a diatom is reportedly lower than those used here;[55] this probably helps prevent spontaneous condensation, or helps produce material with smoother texture. The diatom's use of longer oligoamines may compensate for the diminished reactivity of tertiary oligoamines as pH is reduced.

Diatoms make limited use of quaternary salts, which has not been observed in nearby pairs in the polyamines found in diatoms.[27] It may be that the more reactive moieties studied here are

avoided by diatoms due to their inhibitory effect on metabolic functions. In particular, viologens are widely used as herbicides, so it seems unlikely that diatoms would make use of them from a metabolic standpoint. However, this does not preclude their use for artificial silica growth *in vitro*. In fact, viologen polymers have been studied for this purpose using a conventional sol-gel route.[51]

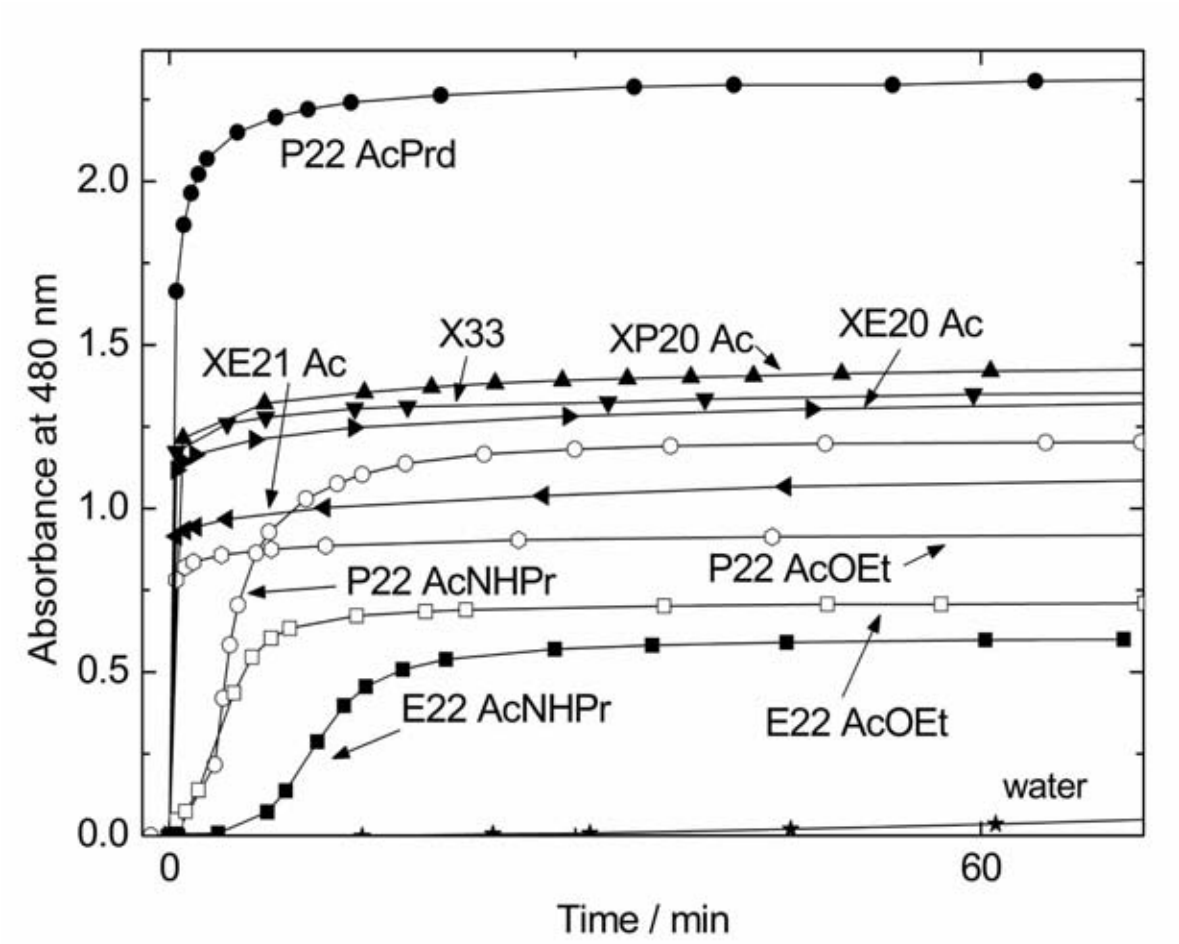

Figure 2.7: Reactivity of phosphate-buffered silicic acid induced by functionalized bis(quaternary ammonium) salts, as measured by the same method as Fig. 2.4. Chemical structures are described in Table 2.2 and 2.3. P22 derivatives are shown by circles, E22 derivatives by squares, and xylyl dibromide derivatives by triangles.

To learn how bis(quaternary ammonium) groups may behave in more complex chemical environments, we have studied the effect of nearby functional groups, particularly those that may enable attachment of these moieties to larger molecules. As shown in Figure 2.7, the reaction product of P22 with ethyl bromoacetate reacts rapidly with silicate and contains active ester groups that, while stable in pH 7 aqueous solutions,[63] can be readily reacted with neat amines to form amides. This could provide a simple way to incorporate bis(quaternary ammonium) into more complex molecules. Amides in this position have a significant effect on reactivity. Propyl amides develop turbidity more slowly than their parent esters, but the final values may be higher or lower. DABCO derivatives were omitted from Figure 2.7 for clarity; the ester rapidly reaches

its final absorbance of 1.0, and the propyl amide trace is close to that of E22 AcOEt. The tertiary amide prepared with P22 EtOAc and pyrrolidine rapidly becomes more than twice as turbid as the ester. This approach is well suited for incorporation into solid-phase combinatorial approaches, which would allow for more thorough screening of the effect of closely neighboring groups on reactivity.

More consistent properties can be obtained when functional groups are spaced farther from the bis(quaternary ammonium) moiety. By acylating asymmetric diamines E20, and P20, and forming a diammonium salt with a xylyl group between them, we can see the effect of isolating an amide by additional methylene groups (see Table 3, XE20 Ac and XP20 Ac). The absorbance curve of XP20 Ac in Figure 2.7 is comparable to the amide-free X33. XP20 Ac has 3 methylene groups separating the amide from the diammonium; the XE20 Ac product, with 2 methylenes, gives similar results. The tertiary amide XE21 Ac shows slightly diminished reactivity compared to the secondary amide. These approaches should allow easy incorporation of silicate-reactive groups into more complex molecules such as surfactants or peptides.

Peptide-bound oligoamines in diatoms are tethered by a lysine residue. The butylene group in lysine, and perhaps the first few amine monomers, may serve as a spacer to isolate amines from interference by groups such as primary amides along the peptide backbone. The strategies noted above should allow incorporation of bis (quaternary ammonium) moieties into artificial peptides that mimic those of diatoms while retaining their exceptional reactivity, perhaps creating a path toward new artificial silica morphologies.

2.4 Summary

Short, highly alkylated diamines constitute a class of minimally complex moieties that strongly accelerate condensation of silicic acid to silica under mild conditions. However, nearby functional groups can modify their effectiveness, so one could expect a larger structure, such as an oligomer, to be more effective in complex environments. Our observations support a previously proposed mechanism in which neighboring cationic amines bring silicate oligomers into a configuration favoring condensation. To this is added a preference for amines with a high degree of alkylation, which we expect would facilitate close association with silicate reactants. The oligoamines in diatoms exhibit these important features.[42] However, they are not known to use bis(quaternary ammonium) salts, which are even more reactive than tertiary diamines and for which we have devised strategies for incorporation into larger molecules. The application of these materials in structured environments, such as surfactant or oligopeptide assemblies, may allow for low-cost and large-scale synthesis of silica structures with specific and programmable nano- and microscale geometries, to a degree of sophistication rivaling that of diatoms.

3.0 IMPACT OF INTERFACIAL CONFINEMENT VIA SURFACTANT MICROEMULSIONS ON SILICA MORPHOLOGY USING AMINE CATALYSTS

3.1 Introduction

Fabrication of inorganic and inorganic-hybrid materials with well-defined size and shape is a topic of considerable current attention.[64,65] In particular, complex silica structures are of interest for a variety of applications, such as transport, catalysis, separation, and drug delivery.[66] In nature, silica formation occurs at neutral to slightly acidic pH under ambient temperatures and pressures with control over product morphology thus far unmatched in the laboratory. Diatoms, unicellular photosynthetic algae, are able to uptake silicic acid from their environment for processing into patterned biosilicas. These diatoms are enclosed in an ornate, mesoporous siliceous shell (frustule) with a species-specific design and morphology spanning multiple length scales.[67] This process is regulated by templating biomolecules via morphosynthesis, wherein the starting materials are spatially confined and the development of emulsions and micelles of a polyamine-containing organic phase are thought to play an active role in directing the growth of these structures.[68] A set of cationic polypeptides ("silaffins") and polyamines have been found to promote and mediate the silica patterning *in vitro*.[69] These co-precipitate with the silica and the frustule is formed with an organic coat tightly incorporated into the silica shell.

The control and patterning that is possible in biogenic silica production has inspired new routes in the laboratory.[70] For instance, the use of linear[71] and dendritic polyamines[72] has recently been documented, alongside a range of smaller amine-containing units.[73] Mediated growth around block co-polypeptide vesicles[74] and the use of individual synthetic peptides[75] have been found to produce hollow and solid silica particles, respectively; such hollow silica spheres have received particular attention for their use in controlled release drug-delivery.[76] One potential advantage of bioinspired synthetic approaches is the avoidance of extreme pH conditions such as those required in common syntheses of the prototypical mesoporous silica MCM-41,[77, 78] which may be important, for example, if molecules intended for encapsulation are themselves sensitive to pH. Examples of the preparation of hollow silica spheres under mild conditions include growth in supercritical CO_2,[79] within block copolymer emulsions in water,[75, 80] around vesicles,[81] and via interfacial[82] and surfactant[83] templating.

We have investigated the incorporation of a branched polyamine, poly(ethyleneimine) (PEI), and monosilicic acid, $Si(OH)_4$ into spherical reverse micelles formed by bis(2-ethylhexyl) sulfosuccinate sodium salt (AOT) in isooctane as a means for bioinspired, controlled silica growth. We found that the reaction conditions within AOT reverse micelles differed from the bulk aqueous solution, allowing for particle growth independent of the initial pH of the amine solution. By altering the size of the water pool from $w_0 = 5$ to 40 ($w_0 = [H_2O]/[AOT]$), various particle sizes and morphologies were generated. Larger reverse micelle sizes ($w_0 \geq 20$) produced trimodal size distributions (ranging from 56 to 500 nm in diameter) of solid silica particles that were found to be mesoporous after calcination, while the use of smaller reverse micelles ($w_0 \leq 10$) resulted in robust, hollow silica shells. These hollow particles are comparably larger, with diameters on the order of 1μm.

3.2 Experimental Details

Bis(2-ethylhexyl) sulfosuccinate sodium salt (AOT) was purchased from Fluka; PEI (poly(ethyleneimine), branched, 1800 MW, 99%, 1:2:1 ratio of primary, secondary, tertiary amines) was purchased from Alfa Aesar; 2,2,4-trimethylpentane (isooctane) was purchased from Sigma-Aldrich; 8-hydroxypyrene-1,3,6-trisulfonic acid (HPTS, or pyranine) was purchased from Invitrogen. Tetramethyl orthosilicate (TMOS, 99%) was purchased from Acros. All chemicals were used as received. Dynamic light scattering (DLS) was performed with a Wyatt Dawn EOS (Wyatt Technologies, Santa Barbara, CA) and particle sizes were determined with QELS Batch 1.0.3.2 software. Scanning electron microscopy (SEM) was performed using a Hitachi 4500 on samples that were drop cast and sputtered with approximately 30 Å of Au/Pd. TEM was performed on a JEOL 1200 or 4000X. UV/vis spectroscopy was performed on a 3802 UNICO spectrometer. Thermogravimetric analysis (TGA) measurements were performed on a Shimadzu TA50. A Shimadzu IR-8400S was utilized in ATR geometry for FTIR measurements. BET surface areas were measured on a Micromeritics porosimeter ASAP 2000 via nitrogen sorption.

Solutions of AOT in isooctane were prepared and stored over activated molecular sieves (4Å, Sigma-Aldrich). Solutions of PEI were prepared in DI water at a range of 0.05 M to 0.025 M (based on primary amine concentration) and adjusted to the desired pH with HCl. Silicic acid solutions were prepared by hydrolysis of 1M TMOS in 1mM HCl at a pH of 3.4 for 15 minutes and used immediately, in accord with previous studies,[95] to reduce the amount of oligomers present versus pure orthosilicic acid. Reverse micelles were prepared by the addition of aqueous PEI or silicic acid solutions to 0.1 M AOT. These were sonicated until the solutions were optically clear, and then monitored by DLS until equilibrium was reached. The PEI-containing reverse micelles were added to the silicic acid-containing reverse micelles and agitated on a shaker overnight. Ratios of amine to silicic acid were controlled using the volumetric ratio of the two respective starting solutions. Typically, a 5:1 volume ratio of the PEI to silicic acid (which is equivalent to a 4:1 molar ratio of silicic acid to PEI) was used, although the range of 1:1 to 10:1 was investigated and gave similar results. The particles obtained were cleaned either by filtering on 20 nm Anotop filters and washing thoroughly with ethanol, or by centrifugation, then washing with ethanol three times.

3.3 Results and Discussion

PEI is structurally comparable to polyamines isolated from *Stephanopyxis turnis* (which contains polyamines consisting of 15-21 N-methylpropyleneimine repeating units attached to putrescine) and *Cylindrotheca fusiformis* (which contains *N*-methylated derivatives of a polypropyleneimine covalently linked to lysine residues).[84] Aggregates of PEI in water and methanol have recently been shown to initiate rapid hydrolytic condensation of tetramethyl orthosilicate (TMOS) with morphologies directed by the PEI concentration.[71] We used $Si(OH)_4$ (obtained by hydrolysis of TMOS, see experimental section) as the silicon source, which occurs naturally in water at 1 to 100 μM (although concentrations within diatoms are known to be much higher during frustule formation) and is thought to be utilized by diatoms for biomineralization.[85] Our initial experiments studied the reaction of PEI in water solution at a range of pH values spanning 6.3 to

11.2. Addition of individual solutions to 1 M $Si(OH)_4$ was found to catalyze precipitation of silica in a number of cases. SEM images of the resulting precipitates (taken after aging for 24 hours) are shown in Figure 3.1. Reaction at basic pH (9 to 11) resulted in the instantaneous condensation of discrete silica particles, whose size and dispersity was found to pH-dependent. Reaction at pH 7 and 8 resulted in the slow deposition of an amorphous silica matrix, and no precipitation was observed at acidic pH.

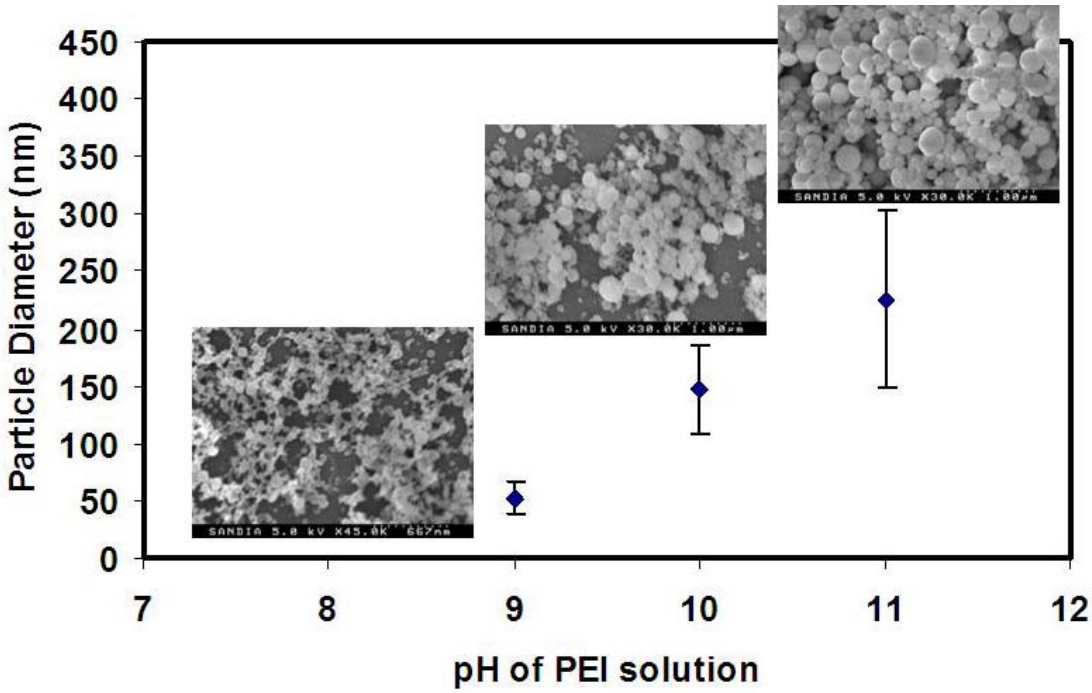

Figure 3.1: Diameter and dispersity of discrete silica particles prepared from aqueous PEI solutions at 0.05 M primary amine concentration and 1M $Si(OH)_4$ at pH 9, 10, and 11 in a 4:1 volume ratio. SEM images of the particles are shown as insets.

We then incorporated PEI and $Si(OH)_4$ into AOT reverse micelles prepared in isooctane. When dissolved in organic solvents, AOT forms thermodynamically stable reverse micelles with a hydrophilic core and hydrophobic alkyl chains extending into the continuous solvent phase. Reverse micelles are known to exchange their contents quickly, with rates of 10^6-10^8 $M^{-1}s^{-1}$,[87] via fusion and redispersion processes, and have been used extensively as confined spaces for the growth of metal and semiconductor nanoparticles.[86] In addition, ammonium hydroxide-catalyzed tetraethyl orthosilicate (TEOS) hydrolysis has been demonstrated in AOT.[87] Solutions of PEI in water (at the same pH values used in the bulk studies) and $Si(OH)_4$ were incorporated into AOT reverse micelles and combined at controlled ratios to initiate the reaction. Initial studies were conducted at $w_0 = 20$, where it is known that a portion of this water is free (not tightly coordinated by the surfactant).[88] The stability of the PEI solubilized in AOT was found to be a function of the initial pH of the PEI solutions. These readily entered the reverse micelles at pH values of 9 or greater to form optically clear solutions, reflecting the low degree of PEI protonation at these pH values[89] and, thus, significant shielding from the anionic sulfonate groups at the reverse micelle surface. Experiments at pH 6-8 required sonication to form stable

reverse micelles (evidenced visually by a loss of turbidity), presumably due to increased electrostatic interaction between AOT and PEI. Dynamic light scattering (DLS) was used to determine the average reverse micelle hydrodynamic radius (R_h) after PEI and $Si(OH)_4$ incorporation. These were sized $R_h = 4.7 \pm 0.8$ nm, 3.5 ± 0.1 nm, and 4.1 ± 0.2 nm for PEI solutions with initial pH = 6.7, 9.0 and 11.2, respectively. The reverse micelles containing silicic acid at $w_0 = 20$ had $R_h = 5.4$ nm $\pm$ 0.4 nm.

Amine-catalyzed condensation of silanol groups leads to the formation of siloxane bonds through a water elimination reaction. This production of additional water dynamically changes the size of the water pool during silica growth, and an observed loss of reverse micelle stability for w_0=20 were found to occur instantly upon addition of PEI/AOT to $Si(OH)_4$/AOT for all PEI solutions at the different pH values investigated. This is evidenced by a transition from a clear to a cloudy solution, and eventual phase separation of water and isooctane. Control experiments with only $Si(OH)_4$/AOT did not show evidence of silica particles after a few days, supporting the proposed catalytic function of the PEI. Interestingly, it was found that similarly-sized silica particles were produced within minutes, regardless of the initial pH of the PEI solution, as shown in Figure 3.2. These SEM images show silica particles that were formed from PEI solutions initially at both pH 9.7 and pH 6.7. Both are characterized by a trimodal distribution of sizes, which size segregate in both 2 and 3 dimensions when dropped from dilute aqueous suspensions onto silicon wafers, resulting in ordered islands of silica particles. The smallest particles (d = 56 ± 6 nm) organize at the bottom, with the intermediate size above (d = 192 ± 31 nm), and the largest particles (> 200 nm) on top. Additionally, the smallest particles often separate from the others to form a self-assembled extended domain, displaying 2D size segregation and ordering. Similar self-organization has been observed once before using a trimodal distribution of polystyrene colloids on chemically-patterned substrates.[90] Currently, the explanation for these three defined size regimes is unknown, but it may have its origins in the destabilization routes of the reverse micelles during silica condensation, which may alter the silica growth rates and corresponding particle sizes.

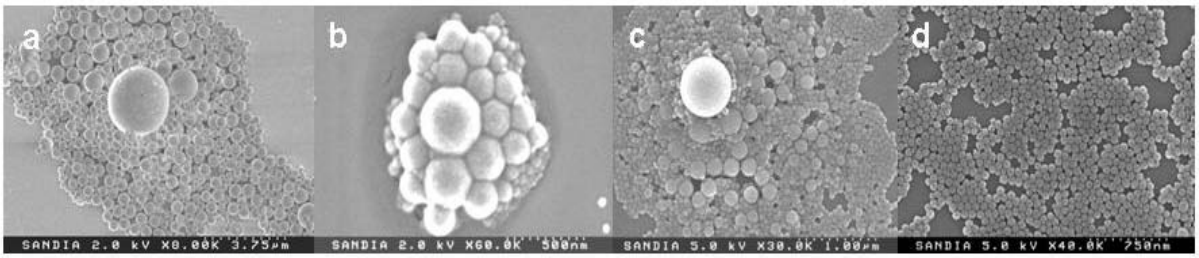

Figure 3.2: SEM images of silica particles prepared in AOT reverse micelles at $w_0 = 20$ using initial PEI solution pH = 9.7 (a,b) and 6.7 (c,d); these self-assemble in 3- (a,b,c) and 2-dimensions (d).

In order to explain the observed phenomena of silica growth in the reverse micelles at neutral to slightly acid pH values (not observed in bulk solution), and the pH-independent particle size distribution obtained, it was necessary to probe the local environment of the water pool inside the reverse micelle. A highly water-soluble pH-sensitive dye, 8-hydroxypyrene-1,3,6-trisulfonic acid

(HPTS, pK_a ~7.3), was utilized to probe the pH of the water confined in the reverse micelle; the phenol and phenoxide forms exhibit distinct absorption bands at 405 and 450 nm, respectively. Aqueous solutions of HPTS were added to AOT in isooctane at a variety of w_0 values, as shown in Figure 3.3. From $w_0 = 5$ to 40, the absorption spectrum was consistent with a pH value of ≥ 9 in bulk water, as determined by the 450/405 ratio.[91] When PEI was added along with HPTS (from $w_0 = 5$ to 40), the same absorption spectrum was observed regardless of the initial pH of the PEI solution. The HPTS absorption changes linearly with PEI concentration, indicating that this is not the result of PEI aggregation. We therefore conclude that the pH in the reverse micelles in this study is dominated by the AOT, resulting in a local pH independent of the initial PEI solution pH.[92]

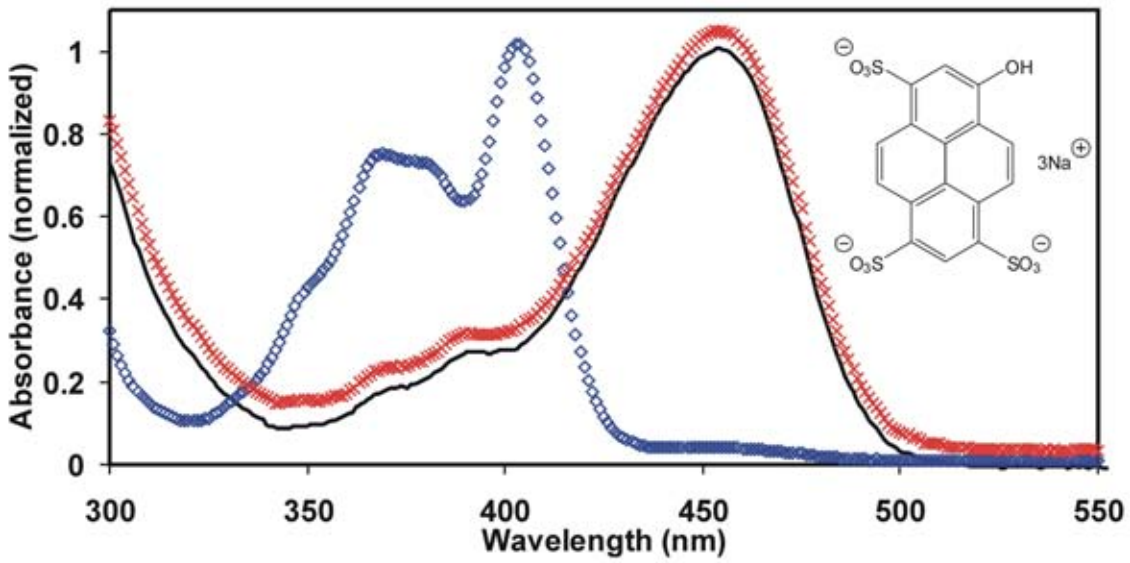

Figure 3.3: Absorption spectra of HPTS in water at pH = 6.5 (diamonds), at initial pH = 6.5 in $w_0 = 20$ reverse micelles (solid line), and at initial pH = 6.5 in $w_0 = 10$ reverse micelles (crosses).

Thermogravimetric analysis (TGA) results indicated a 35 % weight loss upon heating to 500 °C from loss of associated organics. The presence of AOT and PEI within the silica was confirmed by FTIR measurements (see Supporting Information). SEM images of the particles before and after calcination at 500 ºC for 24 hours are shown in Figure 3.4. The particle size does not change, but the surface becomes smoother and a regular pattern of features can be observed. The diameter of the surface features corresponds to approximately 20 nm, which is of a similar size to the original reverse micelles (d = 9.4 nm). This suggests that the initial precipitated particles are formed by aggregation of smaller silica particles in the reverse micelles via micellar exchange, followed by further condensation through siloxane bond formation and co-precipitation of the PEI with the silica. Additionally, the nitrogen sorption isotherm of the calcined particles is characteristic of mesoporous silica,[93] with an increase in surface area from 223 to 693 m^2g^{-1} after calcination (see Supporting Information). This suggested growth mechanism and resulting particle porosity is reminiscent of the hypothesized dynamic nature of

frustule formation, whereby flocculation and intimate connection of nanospheres affords hard cell walls and mesoporous shell structures.[21]

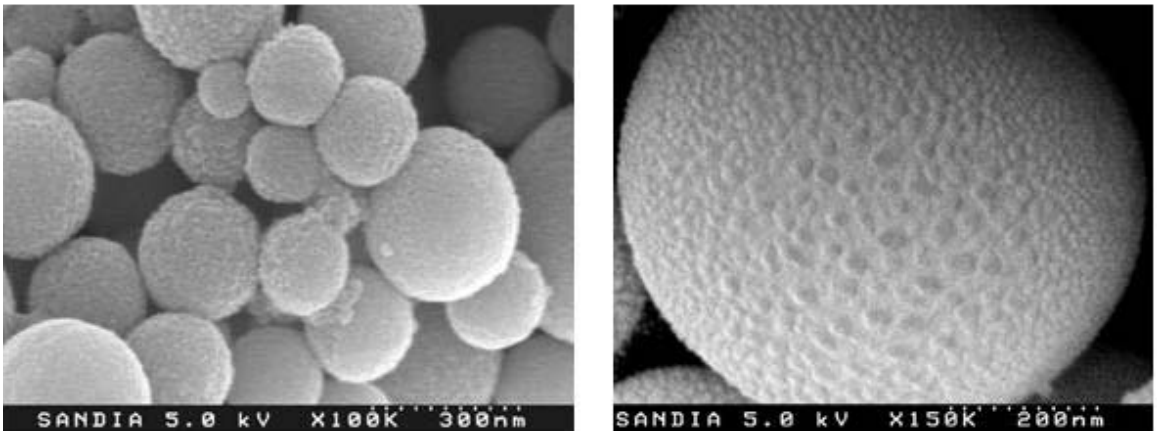

Figure 3.4: SEM images of particles prepared at $w_0 = 20$ before (left) and after (right) calcination at 500ºC. The typically rough nature of the surfaces before heating is evident. The surfaces become smoother and a regular array of nano-sized features (approximately 20nm in diameter) is revealed after calcination.

We also investigated the use of smaller water pools by decreasing the w_0. PEI was readily solubilized in AOT reverse micelles at $w_0 = 10$. Solutions of PEI at pH 6.7 yielded reverse micelles with $R_h = 2.4 \pm 0.1$ nm and $Si(OH)_4$-containing reverse micelles at $w_0 = 10$ had $R_h = 4.3 \pm 0.3$ nm.. Silica particles formed upon combination of the two reverse micelle solutions, although (in contrast to $w_0 = 20$) the majority of the particles formed at $w_0 = 10$ were larger and hollow, as discussed below. The amount of water produced from the condensation reaction at $w_0 = 10$ is small enough for the reverse micelles to maintain their structure throughout, thus allowing the only contact of individual silica units to occur by micellar exchange. The size of the reverse micelle is known to affect the attractive interactions between water pools as smaller w_0 values result in slower growth rates due to decreased coalescence between particles.[86] Additionally, the occupancy number[94] of the precursors is significantly decreased, reducing the number of nuclei for particle growth. This is consistent with observations for metal nanoparticle growth in AOT reverse micelles, whereby smaller particles are formed when the reverse micelle exchange rates are greater and the number of nuclei are larger.[87] The occupancy numbers for PEI in our experiments were found to be ~5 and ~33 PEI/AOT reverse micelle for $w_0 = 10$ and $w_0 = 20$, respectively. Decreasing the PEI occupancy number of $w_0 = 20$ reverse micelles alone did not result in hollow particles, consistent with the suggested destabilization of these reverse micelles by water generated *in-situ* as the dominant factor for the morphological differences.

We believe that the slower exchange rates and smaller number of silica oligomer nuclei for the $w_0 = 10$ case results in the templating of hollow spheres by particle-particle interaction that continues until reactants are consumed, resulting in the formation of intact hollow spheres alongside a population of partially formed rings and spheres. DLS results indicate the reverse micelles are stable after silica formation (approximately 15 minutes, final $R_h = 4.3$ nm), supporting the water-pool exchange route described and suggesting that other potential events, such as formation of larger templates for the hollow spheres, are not important. As for the $w_0 =$

20 case, these results are pH-independent. SEM images of both silica rings and hollow spheres (some cracked during the cleaning process and/or vacuum conditions) are shown in Figure 3.5. These hollow shells remain stable after calcination at 500°C. TEM images (Figure 3.5) reveal a clear distinction between the hollow spheres and smaller, solid particles formed at $w_0 = 10$ and $w_0 = 20$, respectively. Finally, water pools as small as $w_0 = 5$ were investigated. Silica production was found to be inhibited at these values, presumably as the water molecules are tightly coordinated by the sulfonate groups and sodium ions[87] which are more substantially confined with few polymers per micelle. As a result, only a small number of hollow spheres formed, supporting the model proposed above for smaller w_0 values.

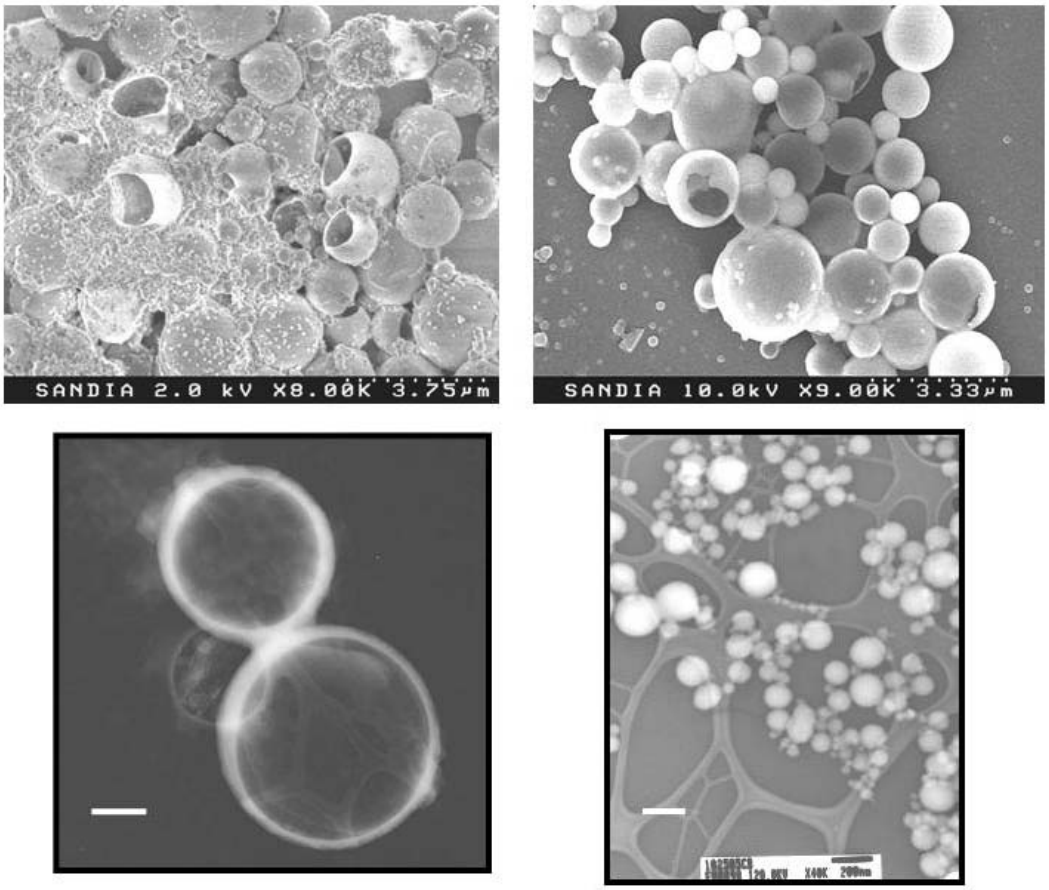

Figure 3.5: SEM images (top) of hollow silica rings (left) and particles (right) prepared at $w_0 = 10$. TEM images (bottom) of hollow particles prepared at $w_0 = 10$ (left, scale bar = 500 nm) and solid particles prepared at $w_0 = 20$ (right, scale bar = 200 nm) shown for comparison.

3.4 Summary

In conclusion, we have presented a bioinspired synthetic procedure that can be readily tuned to produce various silica particle morphologies and sizes from a wide range of initial pH values. This was accomplished by incorporation of PEI and $Si(OH)_4$ into AOT reverse micelles, where

the buffering-like nature of the reverse micelles allows for growth from near-neutral aqueous solutions of PEI. Condensation of $Si(OH)_4$ eliminates water, which presumably dynamically alters the structure of the reverse micelles during particle growth. With larger water pools, this interrupts the reverse micelles to form emulsions and a trimodal size distribution of silica particles results, which can self-assemble in 3D on silicon surfaces. These mesoporous particles are formed via coalescence of smaller particles and co-precipitation of PEI, a process reminiscent of silica growth in diatoms. Reverse micelles with smaller water pools remain stable throughout the silica condensation to allow for growth of larger hollow silica particles, potentially via the slower micellar exchange rate and fewer nuclei present.

4.0 REFERENCES

[1] John, V.T.; Simmons, B.A.; McPherson, G.L.; Bose, A. **Recent developments in materials synthesis in surfactant systems.** Current Opinion in Colloid & Interface Science (2002), 7(5,6), 288-295.

[2] Wetherbee, R. **Biomineralization. The diatom glasshouse**. Science (2002 Oct 18), 298(5593), 547.

[3] Gonzalez-McQuire, R.; Chane-Ching, J.Y.; Vignaud, E.; Lebugle, A.; Mann, S. **Synthesis and characterization of amino acid-functionalized hydroxyapatite nanorods.** Journal of Materials Chemistry (2004), 14(14), 2277-2281.

[4] Hildebrand, M. **Biological processing of nanostructured silica in diatoms.** Progress in Organic Coatings (2003), 47(3-4), 256-266.

[5] Kröger, N.; Bergsdorf, C.; Sumper, M. **Frustulins – Domain conservation in a protein family associated with diatom cell walls.** Eur. J. Biochem. (1996) 239259-264.

[6] Kröger, N.; Lehmann, G.; Rachel, R.;Sumper, M. **Characterization of a 200-kDa diatom protein that is specifically associated with a silica-based substructure of the cell wall.** Eur. J. Biochem. (1997) 250, 99-105.

[7] Poulsen, N.; Sumper, M,; Kröger, N. **Biosilica formation in diatoms: Characterization of native silaffin-2 and its role in silica morphogenesis.** Proceedings of the National Academy of Sciences of the United States of America (2003), 100(21), 12075-12080.

[8] Kröger, N.; Wetherbee, R. **Pleuralins are involved in theca differentiation in the diatom Cylindrotheca fusiformis.** Protist (2000), 151(3), 263-273.

[9]Poulsen, N.; Kröger, N. **Silica Morphogenesis by Alternative Processing of Silaffins in the Diatom Thalassiosira pseudonana**. (2004) J. Biol. Chem., 279, 42993 - 42999

[10] Kröger N.; Deutzmann R.; Bergsdorf C.; Sumper, M. **Species-specific polyamines from diatoms control silica morphology**. Proc Nat'l Acad Sci. (2000) 97, 14133-14138

[11] Kröger N.; Deutzmann R.; Sumper, M. **Polycationic peptides from diatom biosilica that direct silica nanosphere formation.** Science (1999) 286, 1129-1132

[12] Kröger, N, S. Lorenz, E. Brunner, and M. Sumper, **Self-assembly of highly phosphorylated silaffins and their function in biosilica morphogenesis.** Science (2002) 298, 584

[13] Pickett-Heaps, J.; Schmid, A-MM.; Edgar, L.A. **The cell biology of diatom valve formation**. In: Round FE, Chapman DJ (eds) Progress in Pycological Research, (1990) vol 7. Biopress Ltd., Bristol

[14] Clarson, S.J.; Whitlock, P.W.; Patwardhan, S.V.; Brot, L.L.; Naik, R.R.; Stone, M.O. **Synthesis of silica nanostructures at neutral pH using catalytic polypeptides.** Polymeric Materials Science and Engineering (2002), 86, 81.

[15] Brett, L.L.; Naik, R.R.; Pikas, D.J.; Kirkpatrlck, S.M.; Tomlin, D.W.; Whitlock, P.W.; Clarsen, S.J.; Stone, M.O. **Ultrafast holographic nanopatterning of biocatalytically formed silica.** Nature (2001), 413(6853), 291-293.

[16] Knecht, M.R.; Wright, D.W. **Amine-terminated dendrimers as biomimetic templates for silica nanosphere formation.** Langmuir (2004), 20(11), 4728-4732.

[17] Sumper, M.; Lorenz, S.; Brunner, E. **Biomimetic control of size in the polyamine-directed formation of silica nanospheres.** Angewandte Chemie, International Edition (2003), 42(42), 5192-5195.

[18] A. Falciatore and C. Bowler, *Ann. Rev. Plant Bio.* 2002, **53**, 109.

[19] M. Hildebrand, E. York, J. I. Kelz, A. K. Davis, L. G. Frigeri, D. P. Allison and M. J. Doktycz, *J. Mater. Res.* 2006, **21**, 2689.
[20] I. Park, Z. Wang and T. J. Pinnavaia, *Chem. Mater.* 2005, **17**, 383.
[21] F. Schuth, *Ann. Rev. Mater. Res.* 2005, **35**, 209.
[22] N. Kroger, R. Deutzmann and M. Sumper, *Science* 1999, **286**, 1129.
[23] N. Kroger, R. Deutzmann, C. Bergsdorf and M. Sumper, *Proc. Nat. Acad. Sci.* 2000, **97**, 14133.
[24] N. Kroger, R. Deutzmann and M. Sumper, *J. Biol. Chem.* 2001, **276**, 26066.
[25] M. Sumper and N. Kroger, *J. Mater. Chem.* 2004, **14**, 2059.
[26] M. Sumper and E. Brunner, *Adv. Funct. Mater.* 2006, **16**, 17.
[27] M. Sumper and G. Lehmann, *ChemBioChem* 2006, **7**, 1419.
[28] Nicole Poulsen and Nils Kroger, *J. Biol. Chem.* 2004, **279**, 42993.
[29] T. Mizutani, H. Nagase, N. Fujiwara and H. Ogoshi, *Bull. Chem. Soc. Jpn.* 1998, **71**, 2017.
[30] T. Mizutani, H. Nagase and H. Ogoshi, *Chem. Lett.* 1998, 133.
[31] T. Coradin and J. Livage, *Coll. Surf. B.* 2001, **21**, 329.
[32] M. Sumper, S. Lorenz and E. Brunner, *Angew. Chem. Int. Ed.* 2003, **42**, 5192.
[33] V. V. Annenkov, S. V. Patwardhan, D. Belton, E. N. Danilovtseva and C. C. Perry, *Chem. Comm.* **2006**, 1521.
[34] K. M. Delak and N. Sahai, *Chem. Mater.* 2005, **17**, 3221.
[35] S. M. Jones, *J. Noncryst. Solids* 2001, **291**, 206.
[36] K. M. Roth, Y. Zhou, W. Yang and D. E. Morse, *J. Am. Chem. Soc.* 2005, **127**, 325.
[37] P. T. Tanev, Y. Liang and T. J. Pinnavaia, *J. Am. Chem. Soc.* 1997, **119**, 8616.
[38] P. T. Tanev and T. J. Pinnavaia, *Science* 1996, **271**, 1267.
[39] R. R. Naik, P. W. Whitlock, F. Rodriguez, L. L. Brott, D. D. Glawe, S. J. Clarson and M. O. Stone, *Chem. Comm*. 2003, 238.
[40] T. Coradin, O. Durupthy and J. Livage, *Langmuir* 2002, **18**, 2331.
[41] K. Lutz, C. Groger, M. Sumper and E. Brunner, *Phys. Chem. Chem. Phys*. 2005, **7**, 2812.
[42] S. V. Patwardhan and S. J. Clarson, *Silicification and biosilicification*, 2002, **1**, 207.
[43] C. A. Bauer, D. B. Robinson and B. A. Simmons, *Small* 2007, **3**, 58.
[44] M. R. Knecht and D. W. Wright, *Langmuir* 2004, **20**, 4728.
[45] D. J. Belton, S. V. Patwardhan and C. C. Perry, *J. Mater. Chem*. 2005, **15**, 4629.
[46] D. Belton, S. V. Patwardhan and C. C. Perry, *Chem. Comm*. **2005**, 3475.
[47] D. Belton, G. Paine, S. V. Patwardhan and C. C. Perry, *J. Mater. Chem*. 2004, **14**, 2231.
[48] D. H. W. Hubert, M. Jung, P. M. Frederik, P. H. H. Bomans, J. Meuldijk and A. L. German, *Adv. Mater.* 2000, **12**, 1286.
[49] H.-P. Hentze, S. R. Raghavan, C. A. McKelvey, E. W. Kaler, *Langmuir* 2003, **19**, 1069.
[50] Y. Jia, G. M. Gray, J. N. Hay, Y. Li, G.-F. Unali, F. L. Baines and S. P. Armes, *J. Mater. Chem.* 2004, **15**, 2202.
[51] M. J. Adeogun and John N. Hay, *Polym. Intl.* 1996, **41**, 123.
[52] S. D. Kinrade, R. J. Hamilton, A. S. Schach and C. T. G. Knight, J. Chem. Soc., Dalton Trans. 2001, 961.
[53] S. D. Kinrade, A. M. E. Gillson and C. T. G. Knight, *J. Chem Soc., Dalton Trans.* 2002, 307.
[54] K. Thamatrakoln and M. Hildebrand, *J. Nanosci. Nanotech.* 2005, **5**, 158.
[55] E. G. Vrieling, W. W. C. Gieskes and T. P. M. Beelen, *J. Phycol.* 1999, **35**, 548.
[56] R. K. Iler, The Chemistry of Silica, Wiley-Interscience, NY, 1979.
[57] J. L. Trompette and M. Meireles, *J. Coll. Interf. Sci.* 2003, **263**, 522.

[58] P. Schindler and H. R. Kamber, *Helv. Chim. Acta* 1968, **51**, 1781.
[59] C. C. Harrison and N. Loton, *J. Chem. Soc., Faraday Trans.* 1995, **91**, 4287.
[60] D. H. Aue, H. M. Webb and M. T. Bowers, *J. Am. Chem. Soc.* 1976, **98**, 318-329.
[61] R. Zana and J. Xia, ed. Gemini Surfactants (Series: Surfactant Science, v. 117), New York: Marcel Dekker, 2003.
[62] R. Ryoo, I.-S. Park, S. Jun, C. W. Lee, M. Kruk and M. Jaroniec, *J. Am. Chem. Soc*. 2001, **123**, 1650; R. Atkin, V. S. J. Craig, E. J. Wanless and S. Biggs, *J. Phys. Chem. B* 2003, **107**, 2978; M. Benjelloun, P. Van Der Voort, P. Cool, O. Collart and E. F. Vansant, *Phys. Chem. Chem. Phys.*, 2001, **3**, 127.
[63] P. Haberfield and D. Fortier, *J. Org. Chem.* 1983, **48**, 4554.
[64] Castelvetro, V.; De Vita, C. *Adv. Colloid Int. Sci.* **2004**, *108-109*, 167-185.
[65.] Mann, S.; Ozin, G. A. *Nature* **1996**, *382*, 313-318.
[66] a.) Silicon and Siliceous Structures in Biological Systems, ed. T. L. Simpson and B. E. Volcani, Springer-Verlag, New York, 1981. b.) Drum, R. W.; Gordon, R. *Trends Biotechnol.* **2003**, *21*, 325-328.
[67] The Diatom: Biology and Morphology of the Genera, F.E. Round, R.M. Crawford, and D.G. Mann, Cambridge University Press, Camridge, 1990.
[68] Sumper, M. *Science* **2002**, *295*, 2430-2433.
[69] a.)Kroger, N.; Deutzmann, R.; Sumper, M. *Science* **1999**, *286*, 1129-1132., b.) Sumper, M.; Kroger, N. *J. Mater. Chem.* **2004**, *14*, 2059-2065. c.) Kroger, N.; Deutzmann, R.; Bergsdorf, C.; Sumper, M. *P. Natl. Acad. Sci. USA* **2000**, *97*, 14133-14138.
[70] a.) Patwardhan, S., Clarson, S. J., Perry, C. C., *Chem. Commun.* **2005**, 1113-1121., b.) Sun, Q. Y.; Vrieling, E. G.; van Santen, R. A.; Sommerdijk, N. A. J. M. *Curr. Opin. Solid St. Mat.* **2004**, *8*, 111-120.
[71] a.) Brunner, E.; Lutz, K.; Sumper, M. *Phys. Chem. Chem. Phys.* **2004**, *6*, 854-857. b.)Yuan, J. J.; Jin, R. H. *Adv. Mater.* **2005**, *17*, 885-888.
[72] Knecht, M. R.; Sewell, S. L.; Wright, D. W. *Langmuir* **2005**, *21*, 2058-2061.
[73] a.) Roth, K. M.; Zhou, Y.; Yang, W. J.; Morse, D. E. *J. Am. Chem. Soc.* **2005**, *127*, 325-330. b.) T. Coradin and J. Livage, Colloids Surf. B, 2001, 21, 329-336. c.) V.V. Annenkov, S.V. Patwardhan, D. Belton, E.N. Danilovtseva, C.C. Perry, Chem. Comm. **2006**, 1521 and references therein.
[74] Jan, J. S.; Lee, S. J.; Carr, C. S.; Shantz, D. F. *Chem. Mater.* **2005**, *17*, 4310-4317.
[75] Cha, J. N.; Stucky, G. D.; Morse, D. E.; Deming, T. J. *Nature* **2000**, *403*, 289-292.
[76] Zasadzinski, J. A.; Kisak, E.; Evans, C. *Curr. Opin. Colloid In.* **2001**, *6*, 85.
[77] Kresge, C. T.; Leonowicz, M. E.; Roth, W. J.; Vartuli, J. C.; Beck, J. S. *Nature* **1992**, *359*, 710-712.
[78] Sayari, A.; Hamoudi, S. *Chem. Mater.* **2001**, *13*, 3151-3168.
[79] Wang, J.; Xia, Y.; Wang, W.; Mokaya, R.; Poliakoff, M. *Chem. Commun.* **2005**, 210-212.
[80] Sun, Q. Y.; Kooyman, P. J.; Grossmann, J. G.; Bomans, P. H. H.; Frederik, P. M.; Magusin, P. C. M. M.; Beelen, T. P. M.; van Santen, R. A.; Sommerdijk, N. A. J. M. *Adv. Mater.* **2003**, *15*, 1097-1100.
[81] Kim, S. S.; Zhang, W.; Pinnavaia, T. J. *Science* **1998**, *282*, 1302.
[82] Fowler, C. E.; Khushalani, D.; Mann, S. *Chem. Commun.* **2001**, 2028-2029.
[83] Tan, B.; Lehmler, H. J.; Vyas, S. M.; Knuston, B. L.; Rankin, S. E. *Adv. Mater.* **2005**, *17*, 2368-2371.
[84] Sumper, M.; Lorenz, S.; Brunner, E. *Angew. Chem. Int. Edit.* **2003**, *42*, 5192-5195. The

authors note that size control of silica nanospheres can be obtained by variations of polyamine/polyanion ratios.

[85] Treguer, P., Nelson, D. M., Vanbennekom, A. J., Demaster, D. J, Leynaert, A., Queguiner, B., *Science*, **1995**, *268*, 375

[86] Cason, J. P.; Miller, M. E.; Thompson, J. B.; Roberts, C. B. *J. Phys. Chem. B* **2001**, *105*, 2297-2302.

[87] Arriagada, F. J.; Osseoasare, K. *J. Colloid. Interf. Sci.* **1995**, *170*, 8-17.

[88] Bagwe, R. P.; Khilar, K. C. *Langmuir* **1997**, *13*, 6432-6438.

[89] Meszaros, R.; Thompson, L.; Bos, M.; de Groot, P. *Langmuir* **2002**, *18*, 6164-6169.

[90] Karakurt, I.; Leiderer, P.; Boneberg, J. *Langmuir* **2006**, *22*, 2415-2417.

[91] Kano, K.; Fendler, J. H. *Biochim. Biophys. Acta*, **1978**, *509*, 289-298.

[92] A buffering-like capacity of AOT has been noted before in aqueous solutions of various pH; this is attributed to the presence of a high concentration of anionic sulfonate groups, which create a negatively charged interface with the water pool (see Hasegawa, M. *Langmuir* **2001**, *17*, 1426-1431). A similar apparent positive pH shift within the water pools of AOT has been observed using a phenol red colorimetric probe; see Menger, F. M.; Yamada, K. J. *J. Am. Chem. Soc.* **1979**, *101*, 6731-6734. For discussion of the behavior of HPTS in reverse micelles, see Kondo, H.; Miwa, I.; Sunamoto, J. *J. Phys. Chem.* **1982**, *86*, 4826-4831.

[93] Djojoputro, H.; Zhou, X. F.; Qiao, S. Z.; Wang, L. Z.; Yu, C. Z.; Lu G. Q. *J. Am. Chem. Soc.* **2006**, *128*, 6320-6321.

[94] $N_{PEI}/N_{micelles}$; $N_{micelles} = V_{PEI\ solution} / (4/3\ \pi\ r^3)$, where r = radius of micelles as determined by dynamic light scattering (DLS). See reference 25.

[95] Sumper, M. *Angew. Chem. Int. Edit.* **2003**, *4*

DISTRIBUTION:

MS9291 Blake Simmons, 08755
MS9292 Todd Lane, 08321
MS9291 Anup Singh, 08321
MS9161 Arthur Pontau, 08750
MS9291 David Robinson, 08755

MS0123 Donna Chavez, (LDRD Office) 01011
MS0899 Technical Library, 09536 (electronic copy)